JACS
JOURNAL OF THE AMERICAN CHEMICAL SOCIETY

Article

pubs.acs.org/JACS

Tryptophan-Accelerated Electron Flow Across a Protein−Protein Interface

Kana Takematsu,[†,#] Heather Williamson,[†,#] Ana María Blanco-Rodríguez,[‡] Lucie Sokolová,[§] Pavle Nikolovski,[†] Jens T. Kaiser,[†] Michael Towrie,[∥] Ian P. Clark,[∥] Antonín Vlček, Jr.,*[,‡,⊥] Jay R. Winkler,*[,†] and Harry B. Gray*[,†]

[†]Beckman Institute, California Institute of Technology, Pasadena, California 91125, United States

[‡]School of Biological and Chemical Sciences, Queen Mary University of London, London E1 4NS, United Kingdom

[§]Institute of Physical and Theoretical Chemistry, Goethe-Universität, 60438 Frankfurt am Main, Germany

[∥]Central Laser Facility, Research Complex at Harwell, Science and Technology Facilities Council, Rutherford Appleton Laboratory, Harwell Oxford, Didcot, Oxfordshire, OX11 0FA, United Kingdom

[⊥]J. Heyrovský Institute of Physical Chemistry, Academy of Sciences of the Czech Republic, Dolejškova 3, CZ-182 23 Prague, Czech Republic

Supporting Information

ABSTRACT: We report a new metallolabeled blue copper protein, **Re126W122Cu^{I}** *Pseudomonas aeruginosa* azurin, which has three redox sites at well-defined distances in the protein fold: Re^{I}(CO)$_3$(4,7-dimethyl-1,10-phenanthroline) covalently bound at H126, a Cu center, and an indole side chain W122 situated between the Re and Cu sites (Re-W122(indole) = 13.1 Å, dmp-W122(indole) = 10.0 Å, Re-Cu = 25.6 Å). Near-UV excitation of the Re chromophore leads to prompt Cu^{I} oxidation (<50 ns), followed by slow back ET to regenerate Cu^{I} and ground-state Re^{I} with biexponential kinetics, 220 ns and 6 μs. From spectroscopic measurements of kinetics and relative ET yields at different concentrations, it is likely that the photoinduced ET reactions occur in protein dimers, **(Re126W122Cu^{I})$_2$** and that the forward ET is accelerated by intermolecular electron hopping through the interfacial tryptophan: *Re//←W122←Cu^{I}, where // denotes a protein−protein interface. Solution mass spectrometry confirms a broad oligomer distribution with prevalent monomers and dimers, and the crystal structure of the Cu^{II} form shows two **Re126W122Cu^{II}** molecules oriented such that redox cofactors Re(dmp) and W122-indole on different protein molecules are located at the interface at much shorter intermolecular distances (Re-W122(indole) = 6.9 Å, dmp-W122(indole) = 3.5 Å, and Re-Cu = 14.0 Å) than within single protein folds. Whereas forward ET is accelerated by hopping through W122, BET is retarded by a space jump at the interface that lacks specific interactions or water molecules. These findings on interfacial electron hopping in **(Re126W122Cu^{I})$_2$** shed new light on optimal redox-unit placements required for functional long-range charge separation in protein complexes.

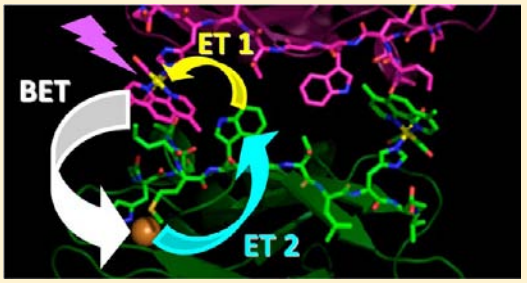

INTRODUCTION

Electron transfer (ET) between metalloproteins is a fundamental step in biological processes such as photosynthesis and respiration.[1] Interprotein ET reactions, which usually occur on μs to ms time scales, can be controlled by gating events that involve exploration of energy landscapes to find productive conformations. A case in point involves dynamic docking of cytochrome b_5 with Zn-myoglobin (Mb), Zn-α-hemoglobin,[2−6] or Zn-cytochrome *c* peroxidase,[6,7] where a Fe^{III}-heme is reduced by a photogenerated Zn(porphyrin) triplet, *^{3}Zn. Dynamic docking allows a redox protein to find the proper reaction partner and maintain electron flow at a rate commensurate with the final substrate transformation.[1]

Much faster (ps−ns) interprotein ET takes place in tightly bound complexes, represented by photosystems I and II of bacterial and plant photosynthesis, where the chlorophyll special pair and nearby redox cofactors are organized in ET active configurations that are fixed in a membrane. This arrangement allows for charge separation in a few ultrafast steps with high conversion efficiency.[8] Similar behavior was demonstrated in an artificial system that featured redesign of the cytochrome b_5//Zn-myoglobin interface by a triple mutation at the Mb surface, thereby enabling formation of a tight complex with two porphyrins near each other.[9−12] Intermolecular ET in the redesigned cytochrome b_5//Zn-myoglobin complex was found to be ultrafast, as it occurs from the short-lived (4 ns) singlet state, *^{1}Zn: reaction times for photoinduced *^{1}ZnMb→Fe^{III}cyt b_5 ET and the corresponding back electron transfer (BET) were 400 and 24 ps, respectively,

Received: July 4, 2013
Published: September 13, 2013

   dx.doi.org/10.1021/ja406830d | *J. Am. Chem. Soc.* 2013, 135, 15515−15525

Scheme 1. Photoinduced ET in $Re^{I}(CO)_3$(dmp)H124X122 azurins (abbreviated Re124X122Cu)[a]

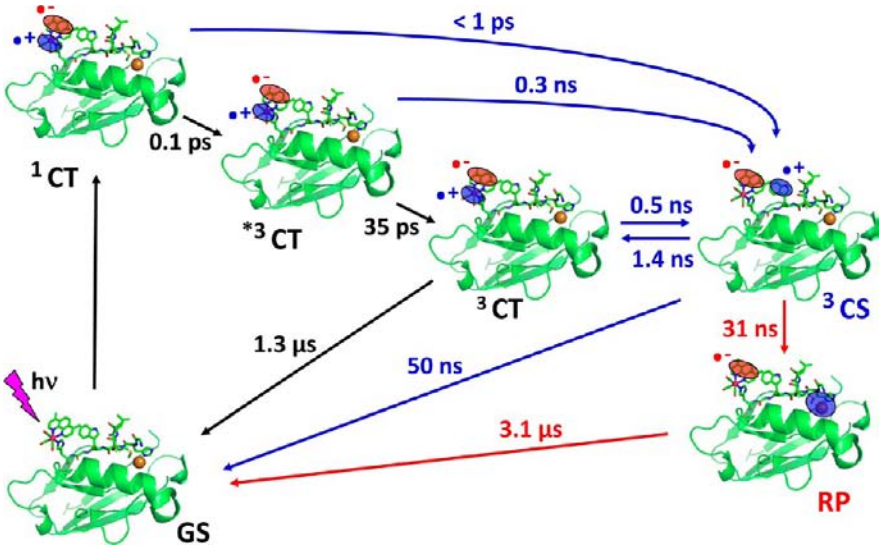

[a]Black: Photocycle of **Re124K122Cu** and **Re124F122Cu**, regardless of the Cu oxidation state, I or II. Black + blue: **Re124W122Cu^{II}** photocycle. Complete scheme (black + blue + red): **Re124W122Cu^{I}** photocycle. ^{*3}CT and ^{3}CT denote hot and relaxed CT states, respectively. The photocycle starts with optical excitation to the CT state $*Re^{II}(CO)_3(dmp^{\bullet-})$H124W122AzCu^{I} followed by several fs/ps/ns ET steps in which W122 is oxidized by $*Re^{II}(CO)_3(dmp^{\bullet-})$, establishing an equilibrium with the charge-separated (CS) state $Re^{I}(CO)_3(dmp^{\bullet-})$H124(W122$^{\bullet+}$) azurin. The oxidized tryptophan intermediate W122$^{\bullet+}$ then undergoes ~30 ns reduction by Cu^{I} over a 11.2 Å distance, forming $Re^{I}(CO)_3(dmp^{\bullet-})$H124W122AzCu^{II} as the redox product (RP). The cycle is completed by ~3 µs $dmp^{\bullet-}$→Cu^{II} BET.[25,26]

with a rate distribution indicating that the photocycle involves a set of reacting configurations.[13] Simulations of this system[14] revealed that Mb surface mutations sharply increase the probability of attaining configurations with short distances between cofactors, where the strongest coupled ET pathways involve direct tunneling between the hemes. This finding is in accord with theoretical work on cyt b_5 self-exchange, which showed that interprotein ET at short distances could be mediated solely by direct cofactor contact, with no involvement of interfacial water molecules in the dominant ET pathways.[15]

Pseudomonas aeruginosa azurin (Az) is a high-potential blue copper protein[1] capable of fast and reversible switching between the Cu^{II} and Cu^{I} oxidation states. Its β-barrel fold is very stable, and its structure is retained upon reducing, removing, or exchanging the Cu^{II} atom, modifying the metal binding site,[16,17] or mutating amino acids in the peptide chain. The combination of fast redox cycling with synthetic flexibility makes azurins promising active components of molecular devices (biomemories or rectifiers).[18−24] Photoactive azurin mutants can be prepared by appending $Re(CO)_3$(diimine) photosensitizers to single surface exposed histidine residues and reducing Cu^{II} to Cu^{I}. Upon near-UV excitation, the metallo-labeled proteins can undergo long-range ET from Cu^{I} to the electronically excited Re^{I} complex (*Re), with the kinetics dependent on the length and nature of the ET pathways.[25−30] Single-step ET between *Re and Cu^{I} ceases to be competitive with the ~1 µs *Re decay as the Cu−Re separation increases. Thus, photoinduced ET was not observed for $Re^{I}(CO)_3$(dmp)-H124X122AzCu^{I} (dmp = 4,7-dimethyl-1,10-phenanthroline, H = histidine, X = lysine (K), phenylanine (F), or tyrosine (Y)), where all other native tryptophan and tyrosine residues were replaced with phenylalanine (All-Phe) and the Re and Cu redox centers are separated by 19.4 Å.[25] ET was found to be (ultra)fast upon inserting tryptophan (X = W122) into the ET pathway, enabling two-step electron hopping (sequential tunneling) through a W122 intermediate (Scheme 1).[25] Electronic coupling in the reactive charge-transfer (CT) state is enhanced by delocalization between the dmp ligand of the Re chromophore and the π-interacting W122(indole), facilitating the primary charge separation step.[26] (Ultra)fast photoreduction of the Re label was thus observed[26] also in the Cu^{II} form, in which the Cu$^{I/II}$ couple does not participate in the photocycle (Scheme 1).

We have investigated a new Re-azurin derivative, $Re^{I}(CO)_3$(dmp)H126W122Az All-Phe (abbreviated **Re126W122Cu^{II}** or **Re126W122Cu^{I}**), where the Re site is two amino acid residues farther away from both W122 and Cu than in the Re124 species, effectively shutting down any direct interaction between the Re(dmp) chromophore and W122. Contrary to our expectations, phototriggered electron flow in **Re126W122Cu^{I}** is as fast as in **Re124W122Cu^{I}**, owing to the presence of a dimer, **(Re126W122Cu^{I})$_2$**, whose structure features a well-coupled intermolecular ET pathway. We report here a rare case of ET acceleration attributable to hopping across a structurally characterized hydrophobic protein−protein interface.

EXPERIMENTAL SECTION

Materials and Sample Preparation. Site-directed mutagenesis K122W/T126H of plasmid *Pseudomonas aeruginosa* Az All-Phe H83Q/Y72F/Y108F/W48F was carried out in two addition cycles using a QuikChange kit (Stratagene) with primers purchased from Invitrogen. Plasmids containing the desired mutant were expressed in BL21(DE3) *E. coli* cells. Protein was collected, purified, and labeled with the Re complex using previously published protocols.[31] 150 µM [$Re(H_2O)(CO)_3$(dmp)](OTf) and 100 µM protein in HEPES buffer were incubated together for 3−4 days at 37 °C and then exchanged into NaP_i buffer. Labeled protein was isolated from unlabeled protein using an IMAC copper-chelating column and purified with a Mono Q anion exchange column. Electrospray ionization mass spectrometry of the final product showed a single peak corresponding to **Re126W122Cu^{II}**. The same procedure was used to prepare and characterize **Re126K122Cu^{II}** and **Re126F122Cu^{II}**.

dx.doi.org/10.1021/ja406830d | J. Am. Chem. Soc. 2013, 135, 15515−15525

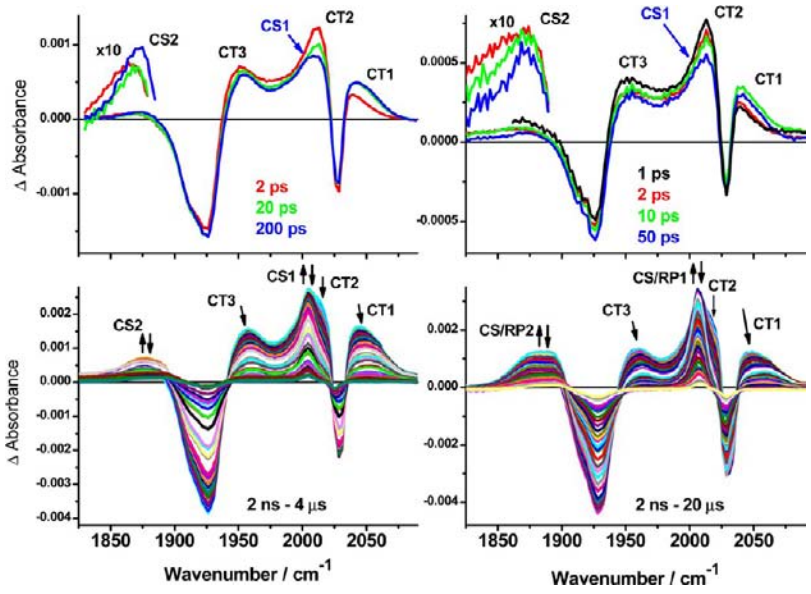

Figure 1. TRIR spectra of ~1 mM **Re126W122Cu^{II}** (left) and **Re126W122Cu^{I}** (right) measured in 50 mM KP_i buffer in D_2O (pD = 7.1) at selected time delays after laser pulse excitation. Top: ps spectra, pumped 355 nm (Cu^{II}) or 400 nm (Cu^{I}), ~50 fs excitation. Experimental points are separated by ~2.2 cm^{-1}. (ps TRIR spectra of **Re126W122Cu^{II}** excited at 400 nm are shown in Figure S1.) Bottom: ns spectra, measured between 1 ns and 50 μs after ~0.7 ns, 355 nm excitation. The spectra evolve in the direction of the arrows. The negative bands (2028, 1926 cm^{-1}) correspond to bleached ground-state absorption. Blue-shifted positive bands (~2040, ~2012 (sh), and 1959 cm^{-1}, labeled CT1, CT2, and CT3) are attributed[45,48−52] to Re→dmp ^{3}MLCT of the Re label. The red-shifted bands at 2003 and 1877 cm^{-1} (labeled CS1 and CS2) are due[25,26,45] to reduced Re label, i.e., $Re^{I}(CO)_3(dmp^{\bullet-})$H126($W122^{\bullet+}$) (CS) for the Cu^{II} species, while for Cu^{I} it corresponds to both CS and $Re^{I}(CO)_3(dmp^{\bullet-})$H126W122AzCu^{II} (RP). No ν(CO) bands were found at lower energies.

Protein Crystallography. Crystals were obtained by sitting-drop vapor diffusion. **Re126W122Cu^{II}** (3 mg/mL in solution of 40 mM imidazole buffer at pH 7.2 with 2 mM NaCl) was mixed with well solution (100 mM imidazole, 100 mM $LiNO_3$, 6.25 mM $CuCl_2$, 25−30% PEG 4000 at pH 7.0−8.0) in a 1:1 ratio (v/v). After 6 months, seed crystals were harvested from two wells (pH 7.4, PEG 27% and pH 7.6, PEG 27%) and used to grow larger crystals over a 4 month period. Crystals were then harvested, coated with a cryoprotectant, and cryogenically stored until data collection. X-ray diffraction data were collected at the Stanford Synchrotron Radiation Laboratory (SSRL) Beamline 12-2 on a DECTRIS Pilatus 6 M detector and processed with XDS[32] and Scala.[33] The structure was solved by molecular replacement with Phaser,[34] using Chain A of PDB 4AZU[35] as a starting model. Coot[36] and Phenix[37] were both used for model building and refinement, with TLS restraints[38] applied in the later refinement cycles. Residual density in some parts was modeled as water. Statistics for data collection, refinement, and validation are provided in Table S1, and the atomic coordinates and structure factors have been deposited in the PDB under entry 4K9J. All molecular graphics were generated using PyMOL.[39]

Spectroscopic Techniques. Laser-induced liquid bead ion desorption mass spectrometry (LILBID-MS)[40] experiments were performed as previously described.[41] Microdroplets of sample solution (diameter 50 μm, volume 65 pL) were produced at 10 Hz by a piezo-driven droplet generator and introduced into vacuum via differential pumping stages. The droplets were irradiated by synchronized 6 ns, mJ mid-IR pulses from a home-built optical parametric oscillator (OPO) using $LiNbO_3$ crystals pumped by a Nd:YAG laser. The OPO wavelength was tuned to the absorption maximum of water stretching vibrations (~3 μm). Preformed protein ions were laser desorbed/ablated from the liquid to the gas phase, where they were mass analyzed in a home-built reflectron time-of-flight (TOF) mass spectrometer with a Daly-type ion detector used for very large biomolecules (m/z up to 10^6). The delay between the laser and the high-voltage ion-accelerating pulses was set at 10 μs. Measurements were performed at two different desorption modes, harsh and soft. Only azurin anions were analyzed. For each experiment, 5 μL of sample solution was loaded into the droplet generator and measured within the first 10 min.

Time-resolved fluorescence and visible transient absorption (TA) experiments on diluted samples (10−100 μM) were performed on a nanosecond laser apparatus with an instrument response time of ~20 ns. Details of the apparatus, along with signal acquisition methods, have been described.[25,42] Samples were excited with 2−4 mJ/pulse of third harmonic light (355 nm) from a Nd:YAG laser (8 ns pulse width, 10 Hz). The probe light for the TA experiments was provided by either a current-pulsed Xe arc lamp (500 nm) or a HeNe laser (632.8 nm). A photomultiplier tube was used for light detection. Data were collected by a LabVIEW program and later processed and fit to multiexponentials in Matlab. Samples were placed in either a 1 mm or 1 cm path length cuvette and stirred with a magnetic bar throughout the experiment. UV−vis spectra of the sample were collected before and after each measurement. Luminescence lifetimes at higher concentrations (0.09−1.5 mM) were determined using a time correlated single photon counting (TCSPC) IBH 5000 U instrument equipped with a cooled Hamamatsu R3809U-50 microchannel plate photomultiplier and an instrument response time of about 100 ps. Samples in a Hellma microcell were excited at 370 nm with an IBH NanoLED-03 diode laser (~100 ps fwhm, 500 kHz repetition rate). Luminescence decays were measured at 560 nm (luminescence maximum) at magic angle between the excitation and emission polarization directions. Data were collected in the 0−900 ns range (971.5 ps/channel).

Time-resolved infrared (TRIR) absorption experiments were performed on the ULTRA instrument[43] at the STFC Rutherford Appleton Laboratory. A titanium sapphire laser-based regenerative amplifier (Thales) produced 800 nm, ~50 fs pulses at a 10 kHz repetition rate. The laser output was split into two parts, one of which was either frequency doubled or used to drive an OPA (Light Conversion, TOPAS) equipped with SHG and SFG units to produce a pump beam at 400 or 355 nm, respectively. The second pumped a TOPAS OPA, yielding signal and idler beams that were difference frequency mixed to generate ~400 cm^{-1} broad mid-IR probe pulses. An optical delay line was used to introduce a delay between the pump and probe beams, and the mid-IR probe spectrum was recorded at a

dx.doi.org/10.1021/ja406830d | J. Am. Chem. Soc. 2013, 135, 15515−15525

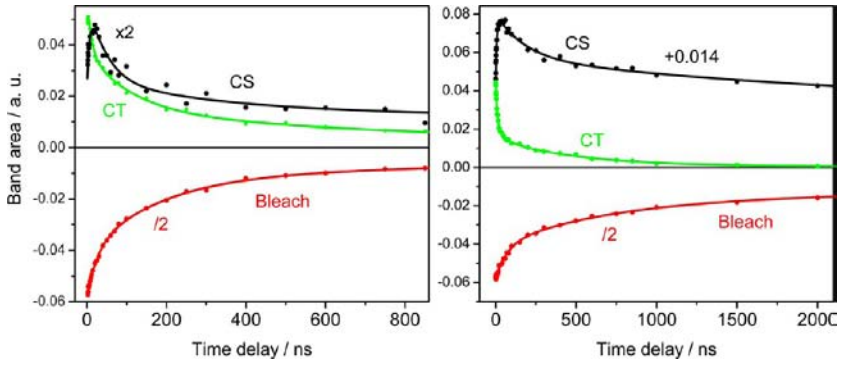

Figure 2. Time-profiles of the IR band areas of CT1, CS2, and 1926 cm^{-1} bleach band areas of **Re126W122Cu^{II}** (left) and **Re126W122Cu^{I}** (right) after 355 nm, 0.7 ns excitation. Experimental conditions as in Figure 1. The bleach areas are divided by 2. The CS areas are multiplied by 2 (left) or vertically offset by +0.014 (right) for clarity.

given time delay using two 128 element HgCdTe detectors (Infrared Associates). Each detector was attached to a spectrograph, which was tuned to a different spectral region with a small region of overlap on each detector to permit acquisition of the full bandwidth. For nanosecond - microsecond measurements, the sample was pumped with 355 nm, 0.7 ns fwhm pulses (AOT, AOT-YVO-20QSP/MOPO) and probed with electronically synchronized 50 fs IR pulses.[44] The sample solutions (0.5−1.0 mM) were placed in a round dip ~0.75 mm deep, drilled into a CaF_2 plate and tightly covered with a polished CaF_2 window. The cell was raster-scanned across the area of the dip in two dimensions orthogonal to the direction of propagation of the laser to prevent laser heating and decomposition of the sample. FTIR spectra were measured before and after the experiment to demonstrate sample stability.

Sample Handling. Concentrations of the starting **Re126-W122Cu^{II}** solutions (~1 mM) were determined by the absorbance at 632 nm, and the samples were diluted to the final concentrations by adding corresponding buffer solutions. Cu^{I} samples were prepared under nitrogen atmosphere by adding either sodium dithionite (TRIR, visible TA, luminescence) or ascorbic acid (visible TA, luminescence) in a buffer solution until discoloration of the Cu^{II} sample. Unreacted reductant was removed with a PD10 column for the optical experiments, while a small dithionite excess remained in the case of TRIR experiments. Cu^{I} samples were further deoxygenated and stored under argon to minimize oxygen contamination in the spectral measurements.

RESULTS AND DISCUSSION

Photoinduced ET. Photoinduced ET reactions of **Re126-W122Cu^{II}** and **Re126W122Cu^{I}** were investigated by a combination of time-resolved spectroscopic techniques over a broad range of sample concentrations (10 μM to 1.5 mM). Measurements on Cu^{II} proteins decouple the long-range Cu^{I} oxidation to investigate the behavior of the Re126W122 moiety alone, while data on Cu^{I} species provide information on the complete photocycle. Luminescence measurements at 560 nm report on decay kinetics of the electronically excited Re^{I} label (*Re, ^{3}CT), and TRIR spectra (Figure 1) show bleaching due to ground-state depletion, blue-shifted bands due to *Re (CT), and red-shifted bands due to reduced Re (CS). Together with time-evolution of the corresponding band areas, TRIR provides structural and kinetics information on the behavior of the Re site (Figure 2). TA of **Re126W122Cu^{I}** at 632.8 and 500 nm reports on the formation and subsequent decay of Cu^{II} and reduced Re, respectively (Figure 3).

Kinetics results of spectroscopic experiments are summarized in Table 1. For both Cu oxidation states, the *Re decay exhibits multiexponential kinetics with lifetimes that are shorter than those of mutants containing K122 or F122 instead of W122.

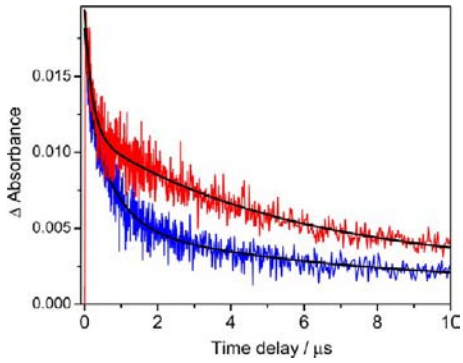

Figure 3. Transient absorption decay of **Re126W122Cu^{I}** (220 μM in 25 mM NaP_i) at 632.8 nm (red) and 500 nm (blue), corresponding to absorbance by Cu^{II} and Re, respectively. Fits in the 20 ns to 100 μs range (black curves): 220 ns (8 mOD amplitude), 6 μs (9 mOD) at 632.8 nm; ~160 ns (4 mOD), 6 μs (4 mOD), 710 ns (8.5 mOD) at 500 nm. The 710 ns lifetime is due to *Re decay of the monomer, while the other components are assigned to the CS/RP states of Re.

TRIR spectra show, in addition to the decaying ^{3}CT bands, a broad band at ~1887 cm^{-1} attributable to the reduced Re chromophore in the ^{3}CS state $Re^{I}(CO)_3(dmp^{\bullet-})(W122^{\bullet+})$ and, for Cu^{I}, also to the reaction product (RP, $Re^{I}(CO)_3(dmp^{\bullet-})(W122)AzCu^{II}$).[25,26,45] The ^{3}CS state is partly formed on a (sub)ps time scale and then rises with a ~7 ns lifetime, followed by a decay whose kinetics depend on the copper oxidation state: 40−55 ns for Cu^{II} and 220 ns and 6 μs for Cu^{I}. TA of **Re126W122Cu^{I}** shows a ≤50 ns rise of the Cu^{II} signal at 632.8 nm, indicating rapid photoxidation of the Cu^{I} site followed by biexponential decay whose lifetimes (220 ns and 6 μs) match those of the CS/RP TRIR band area decay as well as the 500 nm TA decay that combines contributions from *Re and CS.[46,47] The 220 ns and 6 μs kinetics are therefore attributable to BET from $Re^{I}(CO)_3(dmp^{\bullet-})$ to Cu^{II}.

This behavior is qualitatively similar to the well-established[25,26] electron hopping in **Re124W122Cu^{I}** and **Re124-W122Cu^{II}** (Scheme 1), but with several important differences suggesting that photoinduced ET in **Re126W122Cu^{I}** and **Re126W122Cu^{II}** occurs intermolecularly in dimers or oligomers: (1) multiexponential ^{3}CT decay contains an unquenched component whose amplitude increases with decreasing concentration; (2) the maximum intensity of the ^{3}CS TRIR band measured relative to the initial CT3 band intensity is smaller than in the case of **Re124W122Cu^{I}** and **Re124W122Cu^{II}**, indicating a lower ET yield; (3) Cu^{II}

dx.doi.org/10.1021/ja406830d | J. Am. Chem. Soc. 2013, 135, 15515−15525

Table 1. Kinetics Data on Re126 Azurins Obtained from *Re Emission Decay, Time-Resolved Visible Absorption (TA), and Time-Dependent Areas of CT1 and CS2 TRIR Bands[a]

process	emission ^{3}CT decay	TRIR CT1 ^{3}CT decay	TRIR CS2 ^{3}CS rise/decay	emission[e] ^{3}CT decay	TA 633 nm Cu^{II} decay	TRIR CT1 ^{3}CT decay	TRIR CS ^{3}CS rise/decay
		Re126W122Cu^{II}				**Re126W122Cu^{I}**	
dimer ET: *Re^{II}(dmp$^{\bullet-}$)→W122			rise[b] <ps, ~200 ps				rise[b] <ps, ~200 ps
dimer ET: *Re^{II}(dmp$^{\bullet-}$)→W122	3–7 ns[c]	8 ns	rise ~8 ns		rise <50 ns	7–8 ns	rise 5–8 ns
dimer decay: ^{3}CS↔^{3}CT→GS	48 ns	~40 ns	40–55 ns	45 ns		43–45 ns	
dimer BET: Re^{I}(dmp$^{\bullet-}$)→Cu^{II}					220 ns 6000 ns		220–230 ns 6000–6300 ns[f]
monomer decay: ^{3}CT→GS	218 ns	~200 ns		670 ns		670 ns	
Cu^{I} impurity decay: ^{3}CT→GS	~700 ns	700 ns					
dimer <5% ^{3}CS decay[d]			2600–3200 ns				
		Re126F122Cu^{II}				**Re126F122Cu^{I}**	
^{3}CT→GS decay	530 ns			730 ns			
		Re126K122Cu^{II}				**Re126K122Cu^{I}**	
^{3}CT→GS decay	480 ns			730 ns			

[a]Column headings specify the species followed. The leftmost column shows the processes involved (Scheme 2). TRIR kinetics (Figure 2) were determined using band areas, determined by fitting the spectra to a sum of gaussians (see SI). This procedure minimizes effects of spectral shifts and shape changes that accompany the population decay (Figures 1, S3). The 1926 cm^{-1} bleach recovers with multiexponential kinetics that accommodate all the decay lifetimes measured for CT1 and CS2 bands. [b]The apparent rise also involves band narrowing and a small upshift (Figures 1, S1). [c]Determined by TCSPC in the concentration range 90 μM to 1.5 mM. The corresponding amplitude decreases with increasing emission wavelength, suggesting a contribution from a dynamic Stokes shift.[53,54] [d]Very weak long-lived broad CS signal at ~1885 cm^{-1}, presumably due to a species containing deprotonated W122$^{\bullet}$ or to dimer dissociated after ET. [e]Investigated in the 10–30 μM range and at 220 μM. The 45 ns component is more prominent at 220 μM. [f]A very weak persistent signal with a flat maximum around 1887 cm^{-1} present at long time delays. It is presumably due to a species containing deprotonated W122$^{\bullet}$ or dimer dissociation after ET.

Scheme 2. Photoinduced ET in Re^{I}(CO)$_3$(dmp)H126X122 azurins[a]

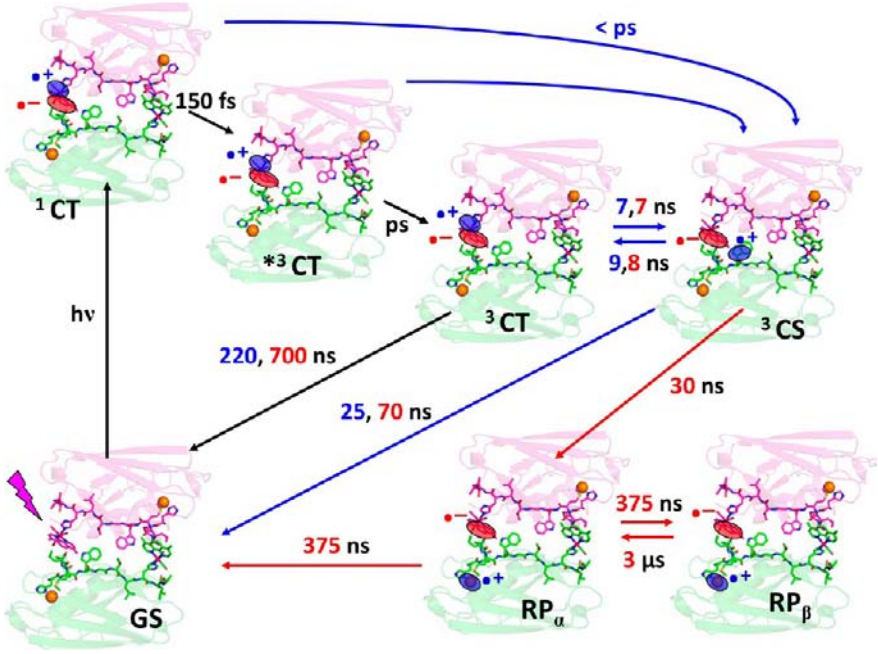

[a]Black: Photocycle of **Re126K122Cu** and **Re126F122Cu** (the Cu oxidation state is I or II). Black + blue: **Re126W122Cu^{II}** photocycle. Complete scheme (black + blue + red): **Re124W122Cu^{I}** photocycle. Lifetime values (k^{-1}) of elementary steps were determined by simulations using a kinetics model, see the text and SI. Values for Cu^{II} and Cu^{I} are shown in blue and red, respectively. *^{3}CT denotes a "hot" state, whose presence and relaxation are manifested by a dynamic shift to higher energies occurring on a tens-of-ps time scale (Figure 1).

formation upon pulsed laser excitation of **Re126W122Cu^{I}** was observed only with protein concentrations >20 μM and its yield increases with concentration; (4) the initial Cu^{II} transient absorbance at 632.8 nm is much smaller for **Re126W122Cu^{I}** than **Re124W122Cu^{I}** measured under comparable conditions; and (5) (sub)picosecond photoreduction of the Re^{I}(CO)$_3$(dmp) label, which was observed in both **Re126W122Cu^{II}** and **Re126W122Cu^{I}** forms, can occur only if Re^{I}(CO)$_3$(dmp) and W122(indole) are in contact prior to excitation, which is not possible within a single molecule.

Based on these observations, we propose that photoinduced ET in (**Re126W122Cu^{II}**)$_2$ and (**Re126W122Cu^{I}**)$_2$ follows a mechanism (Scheme 2) similar to that established[25] for **Re124W122Cu^{I}** (Scheme 1). Regardless of the Cu oxidation state, optical excitation of the Re label produces a singlet CT state, *^{1}Re^{II}(CO)$_3$(dmp$^{\bullet-}$). A small fraction undergoes sub-ps

dx.doi.org/10.1021/ja406830d | J. Am. Chem. Soc. 2013, 135, 15515–15525

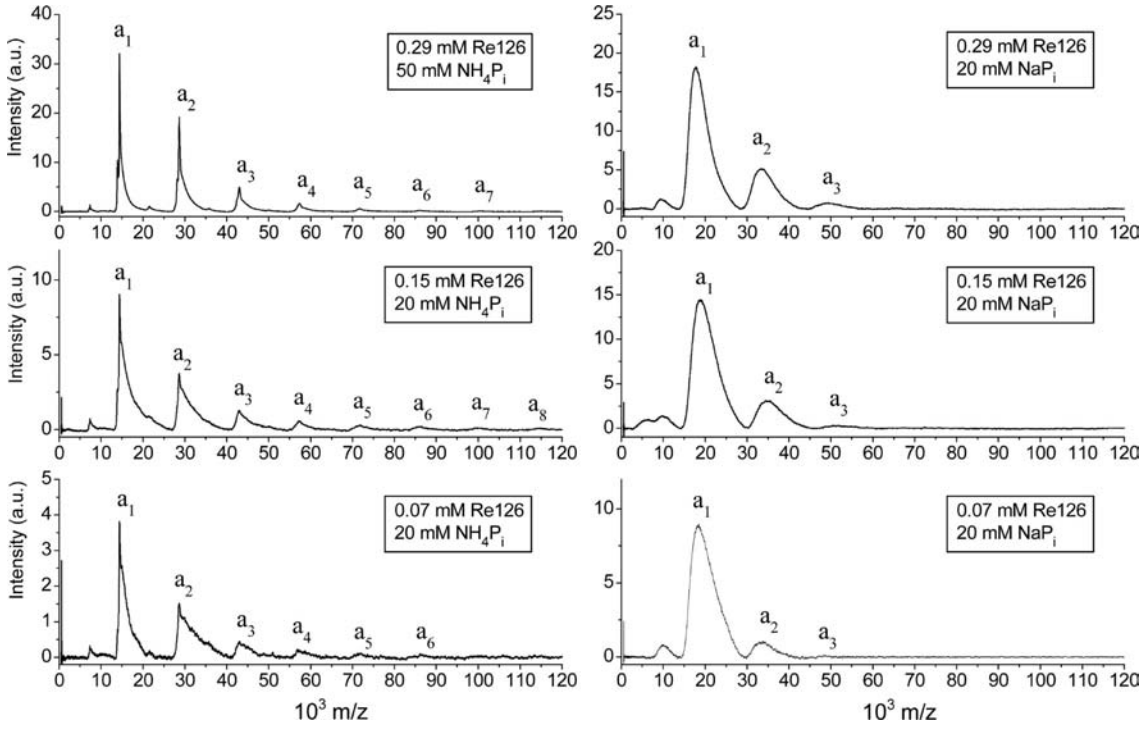

Figure 4. Concentration dependence of LILBID mass spectra of **Re126W122Cu^{II}** in 20 mM NH_4P_i (left) and 20 mM NaP_i (right), measured at soft ionization conditions. The band-shape differences are caused by NH_4^+ decomposition on going to the gas phase, whereas Na^+ ions remain associated with the protein.

reduction by the proximal W122(indole) on the other protein molecule to form the CS state, $Re^I(CO)_3(dmp^{\bullet-})$//$(W122^{\bullet+})$-AzCu, where // denotes the protein−protein interface. (Optical excitation of a W122(indole)→//dmp transition also is possible, although less likely due to a very low oscillator strength.[26]) Most of the ^{1}CT population undergoes ∼150 fs intersystem crossing[47,55] to the ^{3}CT state, $*Re^{II}(CO)_3(dmp^{\bullet-})$. (The skewed shape of the TRIR CT1 band and its small initial shift from the corresponding ground state position (∼+12 cm^{-1}) indicate[26] that ^{3}CT is not pure Re→dmp metal to ligand charge transfer (MLCT) but also involves partial electron transfer from the neighboring W122(indole).) The Re^{II} center in the ^{3}CT state is reduced by intermolecular ET from W122(indole), establishing an equilibrium with the CS state, which also undergoes $Re^I(dmp^{\bullet-})$→//$W122^{\bullet+}$ recombination and, in the case of Cu^I, intramolecular Cu^I→$W122^{\bullet+}$ ET, forming the redox product (RP) $Re^I(CO)_3(dmp^{\bullet-})$//W122Az-$Cu^{II}$. The **(Re126W122Cu^I)$_2$** photocycle is completed by $Re^I(CO)_3(dmp^{\bullet-})$→//$Cu^{II}$ BET. To account for the biexponential BET kinetics, we propose that the initially formed $Re^I(CO)_3(dmp^{\bullet-})$//W122AzCu^{II} ($RP_\alpha$) undergoes BET and simultaneously establishes an equilibrium with another form (RP_β) that either does not undergo BET or does so very slowly. For the equilibrium constant $K \gg 1$, the observed ∼6 μs BET kinetics component arises from slow replenishment of the RP_α population. RP_β formation could involve $W122^{\bullet+}$ deprotonation or fluctuations at the protein−protein interface.

The proposed mechanism (Scheme 2) was simulated by utilizing coupled linear differential equations for time-dependent concentrations of ^{3}CT, CS, RP_α, and RP_β (details in SI). Values for the ^{3}CT decay were determined separately from the unquenched *Re lifetimes measured in dilute solutions. The rate of Cu^I oxidation was assumed to be the same as that determined[25] for **Re124W122Cu^I** since Cu^I→$W122^{\bullet+}$ ET follows the same intramolecular path as in **Re124W122Cu^I**. Identical values of the forward and back rate constants of the RP_α/RP_β conversion were set to reflect the approximately equal amplitudes of the two BET kinetics components in the TA and TRIR experiments. With these assumptions, the simulation yields rate constants for the remaining elementary steps (Scheme 2) that agree with the observed kinetics (Table 1).

The foregoing interpretation of the ET photoreactivity in **Re126W122Cu^{II}** and **Re126W122Cu^I** hinges entirely on the presence of dimers. Next, we will examine possible protein−protein interactions of **Re126W122Cu^{II}** in solutions and crystals.

Solution Behavior of Re126W122Cu^{II}. Unlike other metallolabeled azurins, **Re126W122Cu^{II}** aggregates at concentrations ≥0.75 mM, forming blue flakes that can be redissolved upon gentle warming and agitation. Aggregation is even more pronounced at low pH, and gel formation has been observed at <0.5 mM at low temperatures. The behavior of **Re126-W122Cu^{II}** in solution has been studied by LILBID-MS, a technique able to determine compositions of noncovalent protein complexes and to provide qualitative information on their state in solution,[40,56−58] including unlabeled as well as Re-labeled azurins.[41] LILBID-MS results on **Re126W122Cu^{II}** that are relevant to ET reactivity and the nature of its protein−protein interactions (Figures 4, S4) are as follows: (1) **Re126W122Cu^{II}** forms a broad oligomer distribution in solutions (observable up to about 11-mer at present conditions), with a prominent abundance of monomers and dimers. Unlike the trimer and larger oligomers, dimers are still present at the lowest investigated concentration (70 μM), at which LILBID mass spectra of other Re-labeled and unlabeled azurins show only monomers;[41] (2) peak broadening and a $m/z \approx +6$ kDa shift on going from NH_4P_i to NaP_i buffer indicate protein solvation and association with sodium and phosphate

dx.doi.org/10.1021/ja406830d | J. Am. Chem. Soc. 2013, 135, 15515−15525

ions; and (3) the dimer peak occurs in NaP_i buffer at a mass value that is ~2.9 kDa lower than double the monomer mass, indicating a large protein−protein interface area in the dimer that is deprived of associated buffer ions and solvating water molecules.

Whereas LILBID-MS provides evidence for dimer formation in solution, the concentration dependence of **Re126W122Cu^{II}** luminescence decay kinetics reveals its photophysical effects. Global fitting of decay profiles from t > 20 ns at different concentrations and samples yielded lifetimes of 48 and 218 ns. The latter lifetime is comparable to those measured for unreactive mutants **Re126F122Cu^{II}** and **Re126K122Cu^{II}** (Table 1) and is thus attributable to unreactive monomer **Re126W122Cu^{II}**. (Shortening of the luminescence lifetime of the **Re126W122Cu^{II}** monomer in comparison with **Re126-W122Cu^{I}** (670 ns) is due to energy transfer from *Re to Cu^{II}.) The 48 ns kinetics component is absent in the emission decay of the F122 and K122 mutants. Its presence for **Re126-W122Cu^{II}** documents an active role of the W122 residue in *Re quenching in the absence of the Cu^{I} reducing center. It is attributable to the reactive dimer (**Re126W122Cu^{II}**)$_2$. Accordingly, the relative amplitude of the 48 ns component increases with increasing sample concentration (Figure 5). Its

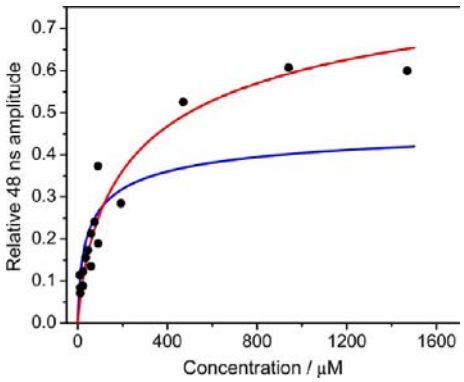

Figure 5. Concentration dependence of the relative amplitude of the 48 ns component of the **Re126W122Cu^{II}** luminescence decay measured in 25 mM NaP_i at 560 nm. The blue and red curves show bests fits using Models 1 (dimerization constant 4.0×10^4 M^{-1}) and 2 (6.1×10^3 M^{-1}), respectively. Data in the concentration ranges 20−90 μM and 0.09−1.5 mM were measured using the ns laser instrument and TCSPC, respectively. For consistency, only the data measured at time delays ≥20 ns were used and fitted globally to triexponential kinetics yielding 48, 217, and 625 ns lifetimes. The latter presumably arose from **Re126W122Cu^{I}** contamination. It disappeared upon addition of an oxidant, $K_3[Co^{III}(oxalate)_3]$ ($E^0(Co^{III/II})$ = 0.57 V) to the sample solution ($E^0(Cu^{II/I})$ = 0.3 V).

concentration dependence was analyzed using two protein−protein interaction models described in the SI. While both models assume a monomer−dimer equilibrium and *Re quenching in the dimer, they differ in the relative orientations of the two **Re126W122Cu^{II}** folds. In Model 1, the interaction is asymmetric, such that Re(dmp) of one molecule can interact with W122 of the other one but not vice versa, so that excitation of only one of the two Re centers results in the quenching process. In Model 2, the interaction is symmetric, and either of the two Re labels will undergo quenching after excitation. Figure 5 shows that Model 2 is more compatible with the concentration dependence of the relative 48 ns luminescence decay amplitude. (Further oligomerization, i.e., addition of monomer(s) to the active dimer, does not substantially alter the behavior predicted by Model 2.)

Crystal Structure of Re126W122Cu^{II}. **Re126W122Cu^{II}** crystallizes in the space group $F222$ with one molecule in the asymmetric unit (Figure 6). The closest distance between the $Re(CO)_3$(dmp) moiety (REQ, atom C3 of the dmp ligand) and W122 indole (C5) is 10.0 Å with an intramolecular Re−Cu distance of 25.6 Å. The closest intramolecular distance between the W122 indole and Cu is 11.0 Å. Examination of interactions between symmetry related molecules reveals an intermolecular distance REQ(C3)-W122′ indole (N_ε) of 3.5 Å (residues in the opposite subunit are designated by a prime). The dmp ligand of REQ and the indole side chain of W122′ are in a T-like orientation; REQ(Re) and Cu′ are separated by 14.0 Å, respectively. The indole rings W122 and W122′ are nearly coplanar and positioned edge-to-edge at 4.5 Å. Water molecules are located mostly at the outer surface of the dimer, confirming the hydrophobic nature of the protein−protein interface. Although protein−protein analysis by the software PISA[59] did not hint at a classical dimerization interface, the orientation of two neighboring **Re124W122Cu^{II}** molecules suggests that the pair can interact in solution through hydrophobic forces as well as indole-dmp donor−acceptor and dispersion interactions.

Intermolecular ET: Electronic Coupling in (Re126-W122Cu^{I})$_2$ and (Re126W122Cu^{II})$_2$. The crystallographically determined protein−protein interaction pattern and distances indicate possible pathways that favor intermolecular over intramolecular ET. Indeed, all intramolecular ET distances are much longer than intermolecular ones (Figure 6). The time constants for both forward and back ET for monomeric **Re126W122** can be calculated using the standard expression for nonadiabatic ET (eq 1; λ = 0.8 eV, $k_0 = 10^{13}$ s^{-1}, r_0 = 3 Å, β = 1.1 $Å^{-1}$, $E^0(Cu^{II/I})$ = 0.3 V vs NHE, $E^0(*Re^{II}(dmp^{\bullet-})/Re^{I}(dmp^{\bullet-}))$ = 1.25 V, $E^0(Re^{I}(dmp^{\bullet-})/Re^{I}(dmp))$ = −1.45 V)[20,60,61]) and were found to be too long in comparison with the experimental data, regardless of the particular mechanism (tunneling or hopping). The rate of intramolecular *Re←Cu^{I} ET in **Re126W122Cu^{I}** is estimated to occur with a time constant of 6.3 ms in the case of single-step tunneling and ≥320 ns for two step *Re←W122←Cu^{I} ET, both much longer than the observed <50 ns Cu^{II} formation. (The 320 ns hopping time is estimated[25,60] using the 10 Å closest dmp-indole intramolecular distance. Using the shortest Re-indole distance (13 Å) gives 8 μs.) The intramolecular BET time constant in **Re126W122Cu^{I}** can be estimated from that observed in **Re124W122Cu^{I}** (3 μs)[25] and the closest Re(dmp)-Cu distances, 23.8 and 15.3 Å, respectively. The estimated value of 34.5 ms is much longer than the observed lifetimes of 220 ns and 6 μs. Hence, only intermolecular ET will be considered in the following discussion.

$$k_{ET} = \frac{2\pi H^2}{\hbar(4\pi\lambda k_B T)^{1/2}}\exp\left[-\frac{(\Delta G^0 + \lambda)^2}{4\lambda k_B T}\right] = k_0\exp\left[-\frac{(\Delta G^0 + \lambda)^2}{4\lambda k_B T}\right] \quad (1a)$$

$$H = H_0\exp\left[-\frac{1}{2}\beta(r - r_0)\right] \quad (1b)$$

As shown in Scheme 2, (**Re126W122Cu^{I}**)$_2$ undergoes *Re//←W122←Cu^{I} ET, completed with Re^{I}(dmp$^{\bullet-}$)//→Cu^{II} BET. The key finding is that intermolecular long-range ET in a

dx.doi.org/10.1021/ja406830d | J. Am. Chem. Soc. 2013, 135, 15515−15525

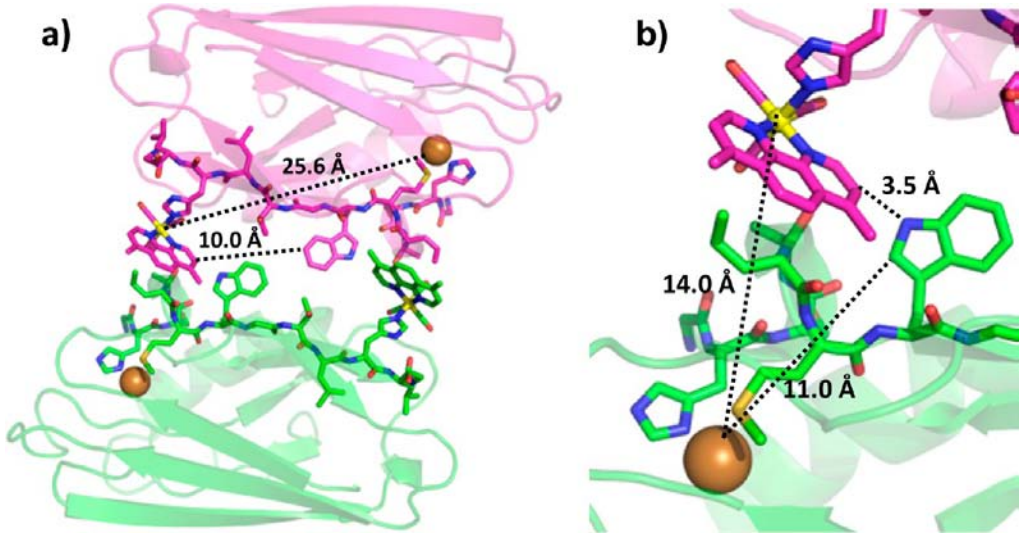

Figure 6. (a) Structure of neighboring **Re126W122Cu^{II}** chains in the unit cell, referred to as a dimer, (**Re126W122Cu^{II}**)$_2$. (b) Closer examination of the dimer interface. The purple and green colors correspond to two interacting molecules of **Re126W122Cu^{II}**, respectively. ET-relevant distances [Å] are specified.

protein complex can be accelerated by hopping across a protein−protein interface. Fast intermolecular *Re//←W122 ET is mediated by electronic coupling between aromatic rings of Re(dmp) and W122(indole) belonging to different azurin folds, which both lie in close proximity (3.5 Å) at the hydrophobic interface. Additional coupling could occur through dmp Me groups.[47,62,63] As a result of these interactions, interfacial ^{3}CT↔CS (i.e., *Re^{II}(dmp$^{\bullet-}$)//W122↔ Re^{I}(dmp$^{\bullet-}$)//W122$^{\bullet+}$) equilibrium is established in a few ns, which is the crucial step in the photocycle as it stores part of the excitation energy and drives long-range Cu^{I} oxidation. The latter step, Cu^{I}→W122$^{\bullet+}$, occurs intramolecularly along the same pathway and with virtually the same rate as in **Re124W122Cu^{I}**.[25,26]

In addition to the hopping mechanism, it is reasonable to consider single-step intermolecular *Re//←Cu^{I} tunneling, for which a lifetime of 18 ns can be estimated assuming that the intermolecular coupling is as strong as that through the single protein fold (eq 1b, r = 14.0 Å, β(Re−Cu) = 1.1 Å^{-1}). The presence of such a competitive reaction, however, is not compatible with the experimental data, as its inclusion in the kinetics model (and varying its time constant from 18 to 200 ns) predicts the *Re decay to occur much faster than the observed ∼7 and 40 ns. The dominance of the hopping mechanism for **Re126W122Cu^{I}** also is supported by the virtually identical ^{3}CT decay and CS rise kinetics observed for Cu^{I} and Cu^{II} species. Rates of hopping vs single-step *Re//←Cu^{I} tunneling can be estimated from ET hopping maps (Figure 8),[25,60] where the ET time is plotted as a function of the driving force for the first tunneling step ($-\Delta G_{first}^{o}$(*Re//←W122)) and of the overall tunneling process ($-\Delta G_{tot}^{o}$(*Re//←Cu^{I})), with black lines enclosing the region in which two-step tunneling is faster than single-step ET. Calculation using parameters relevant for (**Re126W122Cu^{I}**)$_2$ yields a hopping time of 36 ns, in accord with experiment.

The map shown in Figure 8, left, was calculated with all β values equal to 1.1 Å^{-1}, which means that all couplings, including the intermolecular ones, are assumed to be as strong as that mediated by covalent peptide bonds. ET in such a case occurs close to the borderline separating single-step and hopping regions, with single-step tunneling being slightly faster. This assumption, however, is not reasonable for coupling along the single-step Re−Cu intermolecular pathway that involves a 4.5 Å "space jump" that lacks any apparent mediating interactions (Figure 7). Changing β(Re−Cu) to 1.3 Å^{-1} to

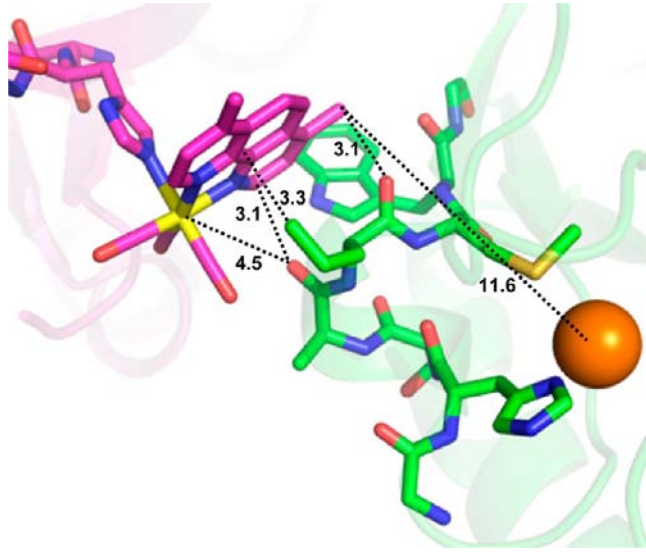

Figure 7. Region of the protein−protein interface in the **Re126W122Cu^{II}** crystal structure relevant to BET and single-step intermolecular tunneling in (**Re126W122Cu^{I}**)$_2$. The shortest distances (in Å) between Re(CO)$_3$(dmp) and the O (Ala119), C(Leu120), and O(Leu120) are shown.

account for weaker coupling modifies the hopping region boundaries in such a way that the value calculated for (**Re126W122Cu^{I}**)$_2$ lies in the hopping region (Figure 8, right). The proximity to the single-step/hopping boundary suggests a possibility of a mixed process whereby both processes would contribute. Such a situation emerged from theoretical analysis of photoinduced ET in the ZnC*c*P//Cyt *c* complex,[12] where only a fraction of ET events involves hopping, depending on the particular Trp environment during

dx.doi.org/10.1021/ja406830d | J. Am. Chem. Soc. 2013, 135, 15515−15525

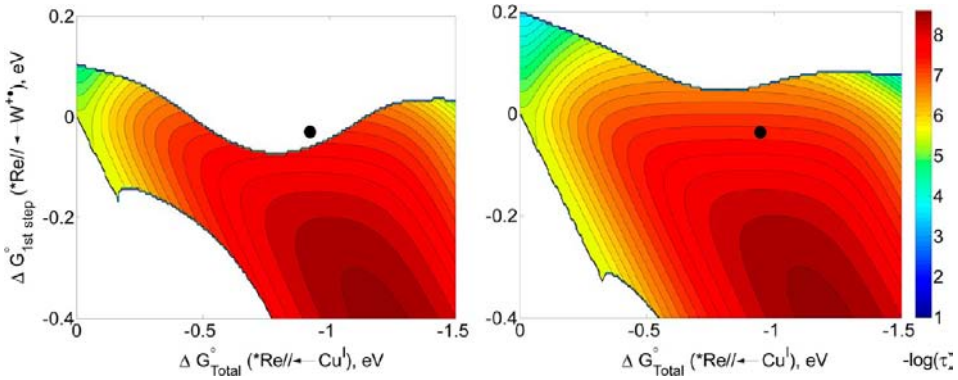

Figure 8. Hopping maps[25,60] calculated for $(\mathbf{Re126W122Cu^{I}})_2$. Left: β(Re-W) = 1.1, β(W-Cu) = 1.1, and β(Re-Cu) = 1.1 Å^{-1}. W-//Re- and W-Cu average distances are 8 and 12 Å, respectively. Right: β(Re-W) = 1.1, β(W-Cu) = 1.1, and β(Re-Cu) = 1.3 Å^{-1}. The black point marks the actual ΔG^0 values for $(\mathbf{Re126W122Cu^{I}})_2$, $-\Delta G^{\circ}_{tot}$ = 0.95 eV, $-\Delta G^{\circ}_{first}$ = 0.030 eV.

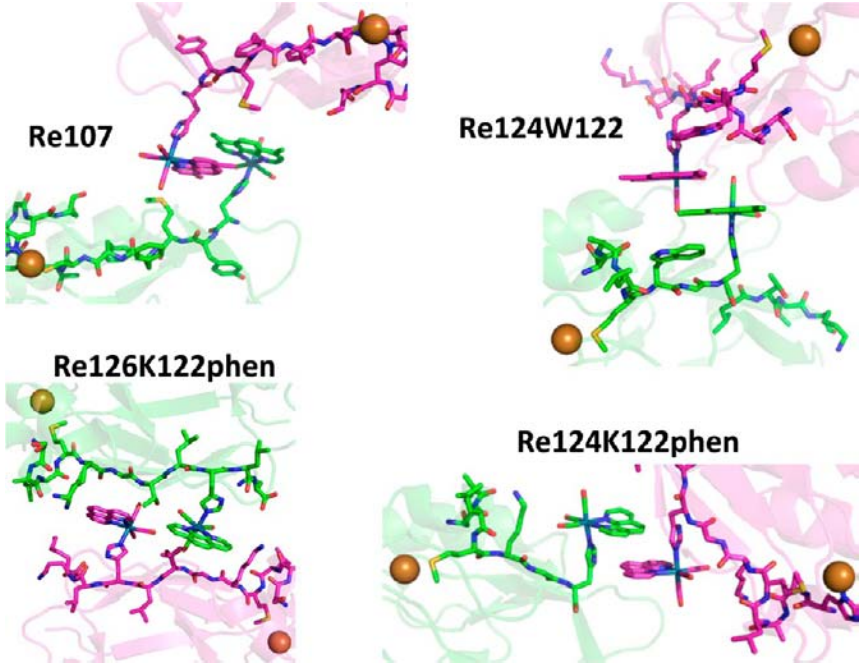

Figure 9. Comparison of protein–protein interactions in crystals of All-Phe Re-labeled azurins. From top-left clockwise: **Re107** = $Re(CO)_3$(dmp)(Q107H)(H83Q)Cu^{II} (PDB: 1I53); **Re124W122** = $\mathbf{Re124W122Cu^{II}}$ (2I7O); **Re124K122phen** = $Re(CO)_3$(phen)(T124H)-(H83Q)Cu^{II} (2I7S); **Re126K122phen** = $Re(CO)_3$(phen)(T126H)(H83Q)Cu^{II} (3IBO).

structural fluctuations. In the case of $(\mathbf{Re126W122Cu^{I}})_2$, we can conclude on kinetics grounds that the hopping mechanism is dominant. This conclusion is further supported by the virtually identical nature and kinetics of early ET steps in the Cu^{II} form that demonstrate a direct reduction of *Re in the absence of any other reducing site except W122.

In contrast to the forward ET pathway, the protein–protein interface in $(\mathbf{Re126W122Cu^{I}})_2$ is not well coupled for $Re^{I}(dmp^{\bullet-})$//→Cu^{II} BET (Figure 7). Based on the 3 μs BET in $\mathbf{Re124W122Cu^{I}}$ over a Cu^{II}-$dmp^{\bullet-}$ distance of 15.3 Å,[25] the BET lifetime in $(\mathbf{Re126W122Cu^{I}})_2$ (11.6 Å) can be estimated (eq 1a) as 51 ns. Both observed BET lifetimes (220 ns, 6 μs) are much longer, suggesting that, despite a short Cu^{II}-$dmp^{\bullet-}$ distance, coupling across a protein–protein interface is weaker than that along the peptide chain in $\mathbf{Re124W122Cu^{I}}$, most likely attributable to the presence of 3–4 Å "space jumps", absence of intermolecular donor–acceptor and H-bonding interactions along the BET pathway as well as to the absence of potentially mediating interfacial H_2O molecules (Figure 7).

Although other Re-labeled azurins also form oligomers in concentrated solutions,[41] the well-coupled interface is a unique feature of the forward ET in $(\mathbf{Re126W122Cu^{II}})_2$. Crystals of All-Phe $\mathbf{Re107Cu^{II}}$ and $\mathbf{Re124K122Cu^{II}}$ show two molecules interacting through dmp–dmp (phen–phen in the latter) π-stacking that connects the two Re labels (Figure 9), precluding intermolecular ET due to long Re-//-Cu distances.[51] The $\mathbf{Re124W122Cu^{II}}$ crystal structure (Figure 9) features a W122(indole)-Re(dmp)//Re(dmp)-W(indole) π-stacked motif[26] that would enable only intramolecular W122-(indole)→*Re(dmp) ET, the interface acting as an insulating barrier. In the case of $\mathbf{Re(phen)126K122Cu^{II}}$, the crystal structure shows the $Re(CO)_3$(phen) unit of one azurin molecule positioned against the peptide chain of a neighboring protein, while the Re sites of the two molecules are laterally separated from each other by amino acid side chains of different

dx.doi.org/10.1021/ja406830d | J. Am. Chem. Soc. 2013, 135, 15515–15525

β-sheets of the two protein folds (Figure 9).[51] In all these cases, the azurin–azurin interface contains several water molecules. A single K122W mutation in **Re126K122Cu^{II}**, which introduces the aromatic amino acid tryptophan, produces a dramatically different **Re126W122Cu^{II}** structure (Figure 6) with a large hydrophobic interface and a pair of Re(dmp)-W122(indole) intermolecular contacts.

CONCLUDING REMARKS

The protein–protein interaction pattern in **(Re126W122Cu^{I})$_2$** and **(Re126W122Cu^{II})$_2$** features a well-coupled intermolecular ET hopping pathway, namely Re(dmp)//W122(indole)-Cu, where the distances between photoredox active units of neighboring molecules are much shorter than respective intramolecular ones (Figure 6). The nature of the *Re^{II}(dmp$^{\bullet-}$)//W122 interfacial interaction is akin to the strongly coupled "direct contact regime" with no bridging water molecules, which emerged from dynamics simulations of cyt b_5//cyt b_5 self-exchange[15] and of the tightly bound Mb-cyt b_5 mutant.[14] The *Re^{II}(dmp$^{\bullet-}$)//W122 coupling is strong enough to mediate sub-ps ET from the ^{1}CT state and to establish a redox equilibrium with the ^{3}CS state Re^{I}(dmp$^{\bullet-}$)//W122$^{\bullet+}$ on a time scale of a few ns (Scheme 2). Unlike the forward reaction, BET is not accelerated by hopping, since Cu^{II} is not able to oxidize tryptophan.

Acceleration of intermolecular ET by hopping across interfaces in protein complexes is rare in nature. One notable case involves hole transfer between two tyrosine residues (Tyr731//Tyr356) at the boundary between α and β subunits of ribonucleotide reductase, although the nature of the coupling is not known.[60,64,65] There are many more examples of intraprotein hopping as documented in photolyases, ribonucleotide reductase, MauG, and in photosystems I and II. Some of these systems were recently analyzed using hopping maps.[60,66] The three-membered "tryptophan wire" in photolyase clearly demonstrates the importance of the right orientation and interaction of indole groups and the chromophore that allow for 30 ps ET across about 15 Å.[67]

It is interesting to note that tryptophan acts as a "rectifier", accelerating ET in only one direction. Re-azurins exemplify the case of forward ET acceleration, whereas selective BET acceleration was observed in (Zn-cyt *c* P)//(cyt *c*) where Fe^{II}-cyt *c* → Zn-cyt *c*P$^+$ BET occurs by hopping through W191 that is positioned close to the cyt *c*P heme but not directly at the protein–protein interface.[7,12,68] A single-docking ET mechanism featuring one-way hopping acceleration through tryptophan placed at a well-coupled hydrophobic protein–protein boundary, documented by our work on **(Re126W122Cu^{I})$_2$**, emerges as a promising strategy to realize long-lived charge separation in protein complexes.

ASSOCIATED CONTENT

Supporting Information

X-ray data collection, refinement statistics, and validation for **Re126W122Cu^{II}**, ps TRIR spectrum of **Re126W122Cu^{II}** after 400 nm excitation, shape analysis of TRIR spectra, dynamic TRIR band shifts, kinetics model of the ET photocycle, harsh-mode LILBID mass spectrum of 0.27 mM **Re126W122Cu^{II}**, analysis of concentration-dependent luminescence intensity of **Re126W122Cu^{II}**. This material is available free of charge via the Internet at http://pubs.acs.org.

AUTHOR INFORMATION

Corresponding Authors

hbgray@caltech.edu
a.vlcek@qmul.ac.uk
winklerj@caltech.edu

Author Contributions

#K.T. and H.W. contributed equally to this work.

Notes

The authors declare no competing financial interest.

ACKNOWLEDGMENTS

We thank Yuling Shen, Crystal Shih, and Jeff Warren (Caltech), respectively, for azurin mutant preparation, preliminary laser measurements, and helpful discussions. Prof. B. Brutschy (Frankfurt) is thanked for discussions on LILBID-MS, and Hana Kvapilová and Jan Sýkora (JH Institute) for their help with some of the TRIR and TCSPC emission experiments. Research at Caltech was supported by NIH (DK019038 to HBG, JRW) and the Arnold and Mabel Beckman Foundation. The TRIR experiments were funded by the STFC Rutherford Appleton Laboratory, Queen Mary University of London, and the Ministry of Education of the Czech Republic grant LH13015. Crystal data were collected on the SSRL Beamline 12-2 through the support of the Caltech Molecular Observatory, funded by the Gordon and Betty Moore Foundation, the Sanofi-Aventis Bioengineering Research Program.

REFERENCES

(1) *Biological Inorganic Chemistry*; Bertini, I., Gray, H. B., Stiefel, E. I., Valentine, J. S., Eds.; University Science Books: Sausalito, CA, 2007.
(2) Liang, Z.-X.; Nocek, J. M.; Huang, K.; Hayes, R. T.; Kurnikov, I. V.; Beratan, D. N.; Hoffman, B. M. *J. Am. Chem. Soc.* **2002**, *124*, 6849.
(3) Liang, Z.-X.; Kurnikov, I. V.; Nocek, J. M.; Mauk, A. G.; Beratan, D. N.; Hoffman, B. M. *J. Am. Chem. Soc.* **2004**, *126*, 2785.
(4) Wheeler, K. E.; Nocek, J. M.; Cull, D. A.; Yatsunyk, L. A.; Rosenzweig, A. C.; Hoffman, B. M. *J. Am. Chem. Soc.* **2007**, *129*, 3906.
(5) Patel, A. D.; Nocek, J. M.; Hoffman, B. M. *J. Am. Chem. Soc.* **2005**, *127*, 16766.
(6) Hoffman, B. M.; Celis, L. M.; Cull, D. A.; Patel, A. D.; Seifert, J. L.; Wheeler, K. E.; Wang, J.; Yao, J.; Kurnikov, I. V.; Nocek, J. M. *Proc. Natl. Acad. Sci. U.S.A.* **2005**, *102*, 3564.
(7) Seifert, J. L.; Pfister, T. D.; Nocek, J. M.; Lu, Y.; Hoffman, B. M. *J. Am. Chem. Soc.* **2005**, *127*, 5750.
(8) Nelson, N.; Yocum, C. F. *Annu. Rev. Plant Biol.* **2006**, *57*, 521.
(9) Xiong, P.; Nocek, J. M.; Griffin, A. K. K.; Wang, J.; Hoffman, B. M. *J. Am. Chem. Soc.* **2009**, *131*, 6938.
(10) Nocek, J. M.; Knutson, A. K.; Xiong, P.; Co, N. P.; Hoffman, B. M. *J. Am. Chem. Soc.* **2010**, *132*, 6165.
(11) Trana, E. N.; Nocek, J. M.; Knutson, A. K.; Hoffman, B. M. *Biochemistry* **2012**, *51*, 8542–8553.
(12) Jiang, N.; Kuznetsov, A.; Nocek, J. M.; Hoffman, B. M.; Crane, B. R.; Hu, X.; Beratan, D. N. *J. Phys. Chem. B* **2013**, *117*, 9129–9141.
(13) Xiong, P.; Nocek, J. M.; Vura-Weis, J.; Lockard, J. V.; Wasielewski, M. R.; Hoffman, B. M. *Science* **2010**, *330*, 1075.
(14) Keinan, S.; Nocek, J. M.; Hoffman, B. M.; Beratan, D. N. *Phys. Chem. Chem. Phys.* **2012**, *14*, 13881.
(15) Lin, J.; Balabin, I. A.; Beratan, D. N. *Science* **2005**, *310*, 1311.
(16) Lancaster, K. M.; Yokoyama, K.; Richards, J. H.; Winkler, J. R.; Gray, H. B. *Inorg. Chem.* **2009**, *48*, 1278.
(17) Lancaster, K. M.; Farver, O.; Wherland, S.; Crane, E. J., III; Richards, J. H.; Pecht, I.; Gray, H. B. *J. Am. Chem. Soc.* **2011**, *133*, 4865.

(18) Bramanti, A.; Pompa, P. P.; Maruccio, G.; Calabi, F.; Arima, V.; Cingolani, R.; Corni, S.; Di Felice, R.; De Rienzo, F.; Rinaldi, R. *Jpn. J. Appl. Phys.* **2005**, *44*, 6864.
(19) Choi, J.-W.; Oh, B.-K.; Kim, Y. J. *Appl. Phys. Lett.* **2007**, *91*, 263902.
(20) Lee, T.; Kim, S.-U.; Min, J.; Choi, J.-W. *Adv. Mater.* **2010**, *22*, 510.
(21) Rinaldi, R.; Biasco, A.; Maruccio, G.; Arima, V.; Visconti, P.; Cingolani, R.; Facci, P.; De Rienzo, F.; Di Felice, R.; Molinari, E.; Verbeet, M. P.; Canters, G. W. *Appl. Phys. Lett.* **2003**, *82*, 472.
(22) Ron, I.; Sepunaru, L.; Itzhakov, S.; Belenkova, T.; Friedman, N.; Pecht, I.; Sheves, M.; Cahen, D. *J. Am. Chem. Soc.* **2010**, *132*, 4131.
(23) Li, W.; Sepunaru, L.; Amdursky, N.; Cohen, S. R.; Pecht, I.; Sheves, M.; Cahen, D. *ACS Nano* **2012**, *6*, 10816.
(24) Sepunaru, L.; Pecht, I.; Sheves, M.; Cahen, D. *J. Am. Chem. Soc.* **2011**, *133*, 2421.
(25) Shih, C.; Museth, A. K.; Abrahamsson, M.; Blanco-Rodriguez, A. M.; Di Bilio, A. J.; Sudhamsu, J.; Crane, B. R.; Ronayne, K. L.; Towrie, M.; Vlček, A., Jr.; Richards, J. H.; Winkler, J. R.; Gray, H. B. *Science* **2008**, *320*, 1760.
(26) Blanco-Rodríguez, A. M.; Di Bilio, A. J.; Shih, C.; Museth, A. K.; Clark, I. P.; Towrie, M.; Cannizzo, A.; Sudhamsu, J.; Crane, B. R.; Sýkora, J.; Winkler, J. R.; Gray, H. B.; Záliš, S.; Vlček, A., Jr. *Chem.—Eur. J.* **2011**, *17*, 5350.
(27) Connick, W. B.; Di Bilio, A. J.; Hill, M. G.; Winkler, J. R.; Gray, H. B. *Inorg. Chim. Acta* **1995**, *240*, 169.
(28) Miller, J. E.; Di Bilio, A. J.; Wehbi, W. A.; Green, M. T.; Museth, A. K.; Richards, J. R.; Winkler, J. R.; Gray, H. B. *Biochim. Biophys. Acta* **2004**, *1655*, 59.
(29) Crane, B. R.; Di Bilio, A. J.; Winkler, J. R.; Gray, H. B. *J. Am. Chem. Soc.* **2001**, *123*, 11623.
(30) Winkler, J. R.; Di Bilio, A. J.; Farrow, N. A.; Richards, J. H.; Gray, H. B. *Pure Appl. Chem.* **1999**, *71*, 1753.
(31) Di Bilio, A. J.; Crane, B. R.; Wehbi, W. A.; Kiser, C. N.; Abu-Omar, M. M.; Carlos, R. M.; Richards, J. H.; Winkler, J. R.; Gray, H. B. *J. Am. Chem. Soc.* **2001**, *123*, 3181.
(32) Kabsch, W. *Acta Crystallogr.* **2010**, *D66*, 125.
(33) Kabsch, W. *J. Appl. Crystallogr.* **1988**, *21*, 916.
(34) McCoy, A. J.; Grosse-Kunstleve, R. W.; Adams, P. D.; Winn, M. D.; Storoni, L. C.; Read, R. J. *J. Appl. Crystallogr.* **2007**, *40*, 658.
(35) Nar, H.; Messerschmidt, A.; Huber, R.; van de Kamp, M.; Canters, G. W. *J. Mol. Biol.* **1991**, *221*, 765.
(36) Emsley, P.; Cowtan, K. *Acta Crystallogr.* **2004**, *D60*, 2126.
(37) Adams, P. D.; Mustyakimov, M.; Afonine, P. V.; Langan, P. *Acta Crystallogr.* **2009**, *D65*, 567.
(38) Painter, J.; Merritt, E. A. *J. Appl. Crystallogr.* **2006**, *39*, 109.
(39) *Pymol: PyMOL Molecular Graphics System*, Version 1.3, Schrödinger, LLC: Cambridge, MA2010.
(40) Morgner, N.; Barth, H.-D.; Brutschy, B. *Austral. J. Chem.* **2006**, *59*, 109.
(41) Sokolová, L.; Williamson, H.; Sýkora, J.; Hof, M.; Gray, H. B.; Brutschy, B.; Vlček, A., Jr. *J. Phys. Chem. B* **2011**, *115*, 4790.
(42) Kuciauskas, D.; Freund, M. S.; Gray, H. B.; Winkler, J. R.; Lewis, N. S. *J. Phys. Chem. B* **2001**, *105*, 392.
(43) Greetham, G.; Burgos, P.; Cao, Q.; Clark, I. P.; Codd, P.; Farrow, R.; George, M. W.; Kogimtzis, M.; Matousek, P.; Parker, A. W.; Pollard, M.; Robinson, D.; Xin, Z.-J.; Towrie, M. *Appl. Spectrosc.* **2010**, *64*, 1311.
(44) Towrie, M.; Parker, A. W.; Vlček, A., Jr.; Gabrielsson, A.; Blanco Rodriguez, A. M. *Appl. Spectrosc.* **2005**, *59*, 467.
(45) Blanco-Rodríguez, A. M.; Towrie, M.; Sýkora, J.; Záliš, S.; Vlček, A., Jr. *Inorg. Chem.* **2011**, *50*, 6122.
(46) Záliš, S.; Consani, C.; El Nahhas, A.; Cannizzo, A.; Chergui, M.; Hartl, F.; Vlček, A., Jr. *Inorg. Chim. Acta* **2011**, *374*, 578.
(47) El Nahhas, A.; Consani, C.; Blanco-Rodríguez, A. M.; Lancaster, K. M.; Braem, O.; Cannizzo, A.; Towrie, M.; Clark, I. P.; Záliš, S.; Chergui, M.; Vlček, A., Jr. *Inorg. Chem.* **2011**, *50*, 2932.
(48) Gamelin, D. R.; George, M. W.; Glyn, P.; Grevels, F.-W.; Johnson, F. P. A.; Klotzbücher, W.; Morrison, S. L.; Russell, G.; Schaffner, K.; Turner, J. J. *Inorg. Chem.* **1994**, *33*, 3246.
(49) Dattelbaum, D. M.; Omberg, K. M.; Hay, P. J.; Gebhart, N. L.; Martin, R. L.; Schoonover, J. R.; Meyer, T. J. *J. Phys. Chem. A* **2004**, *108*, 3527.
(50) Vlček, A., Jr. *Top. Organomet. Chem.* **2010**, *29*, 73.
(51) Blanco-Rodríguez, A. M.; Busby, M.; Ronayne, K. L.; Towrie, M.; Sýkora, J.; Hof, M.; Záliš, S.; Grădinaru, C.; Di Bilio, A. J.; Crane, B. R.; Gray, H. B.; Vlček, A., Jr. *J. Am. Chem. Soc.* **2009**, *131*, 11788.
(52) Blanco-Rodríguez, A. M.; Busby, M.; Grădinaru, C.; Crane, B. R.; Di Bilio, A. J.; Matousek, P.; Towrie, M.; Leigh, B. S.; Richards, J. H.; Vlček, A., Jr.; Gray, H. B. *J. Am. Chem. Soc.* **2006**, *128*, 4365.
(53) Horng, M. L.; Gardecki, J. A.; Papazyan, A.; Maroncelli, M. *J. Phys. Chem.* **1995**, *99*, 17311.
(54) Pospíšil, P.; Sýkora, J.; Takematsu, K.; Hof, M.; Gray, H. B.; Vlček, A., Jr. work in progress.
(55) Cannizzo, A.; Blanco-Rodríguez, A. M.; Nahhas, A.; Šebera, J.; Záliš, S.; Vlček, A., Jr.; Chergui, M. *J. Am. Chem. Soc.* **2008**, *130*, 8967.
(56) Morgner, N.; Kleinschroth, T.; Barth, H.-D.; Ludwig, B.; Brutschy, B. *J. Am. Soc. Mass Spectrom.* **2007**, *18*, 1429.
(57) Morgner, N.; Zickermann, V.; Kerscher, S.; Wittig, I.; Abdrakhmanova, A.; Barth, H.-D.; Brutschy, B.; Brandt, U. *Biochim. Biophys. Acta* **2008**, *1777*, 1384.
(58) Hoffmann, J.; Aslimovska, L.; Bamann, C.; Glaubitz, C.; Bamberg, E.; Brutschy, B. *Phys. Chem. Chem. Phys.* **2010**, *12*, 3480.
(59) Krissinel, E.; Henrick, K. *J. Mol. Biol.* **2007**, *372*, 774.
(60) Warren, J. J.; Ener, M. E.; Vlček, A., Jr.; Winkler, J. R.; Gray, H. B. *Coord. Chem. Rev.* **2012**, *256*, 2478.
(61) Gray, H. B.; Winkler, J. R. *Proc. Natl. Acad. Sci. U.S.A.* **2005**, *102*, 3534.
(62) Kaim, W. *J. Am. Chem. Soc.* **1982**, *104*, 3883.
(63) Jasaitis, A.; Johansson, M. P.; Wikström, M.; Vos, M. H.; Verkhovsky, M. I. *Proc. Natl. Acad. Sci. U.S.A.* **2007**, *52*, 20811.
(64) Stubbe, J.; Nocera, D. G.; Yee, C. S.; Chang, M. C. Y. *Chem. Rev.* **2003**, *103*, 2167.
(65) Reece, S. Y.; Hodgkiss, J. M.; Stubbe, J.; Nocera, D. G. *Philos. Trans. R. Soc., B* **2006**, *361*, 1351.
(66) Warren, J. J.; Winkler, J. R.; Gray, H. B. *Coord. Chem. Rev.* **2013**, *257*, 165.
(67) Lukacs, A.; Eker, A. P. M.; Byrdin, M.; Brettel, K.; Vos, M. H. *J. Am. Chem. Soc.* **2008**, *130*, 14394.
(68) Kang, S. A.; Crane, B. R. *Proc. Natl. Acad. Sci. U.S.A.* **2005**, *102*, 15465.